

000 WEAK BISIMULATION METRIC-BASED REPRESENTATIONS FOR SPARSE-REWARD REINFORCEMENT 001 002 LEARNING 003 004 005

006 **Anonymous authors**

007 Paper under double-blind review
008
009
010
011
012

ABSTRACT

013 Recent studies have shown that bisimulation metrics possess the superiority of
014 essentially extracting the features related to reinforcement learning tasks. How-
015 ever, limited by strict assumptions and the inherent conflict between metrics and
016 sparse rewards, they suffer from serious representation degeneration and even col-
017 lapsed in sparse reward settings. To tackle the problems, we propose a reward-
018 free weak bisimulation metric-based Scalable Representation Learning approach
019 (**SRL**). Specifically, we first introduce the weak bisimulation metric, which by-
020 passes the intractable reward difference, instead leveraging a trainable Gaussian
021 distribution to relax the traditional bisimulation metrics. Particularly, the Gaussian
022 noise creates a flexible information margin for the metric optimization, which mit-
023 igates potential representation collapse caused by sparse rewards. Additionally,
024 due to its pure distribution internally, the metric potentially mitigates representa-
025 tion degeneration resulting from inconsistent computations under strict assump-
026 tions. To tighten the metric, we accordingly consider continuous differences over
027 the transition distribution to enhance the accuracy of the initial transition distri-
028 bution difference, strengthening the extraction of equivalent task features. We
029 evaluate SRL on challenging DeepMind Control Suite, MetaWorld, and Adroit
030 tasks with sparse rewards. Empirical results demonstrate that SRL significantly
031 outperforms state-of-the-art baselines on various tasks. The source code will be
032 available later.
033

1 INTRODUCTION

034 Deep reinforcement learning (DRL) with visual input usually requires learning a low-dimensional
035 state representation from high-dimensional pixels to serve downstream policy learning (Stooke et al.,
036 2021; Ze et al., 2024). Recent literature has demonstrated that the quality of state representation is
037 crucial to the efficiency and performance of policy learning (Tang et al., 2023; Zheng et al., 2024),
038 and the ideal representation should provide sufficient non-redundant information for DRL decision-
039 making (Liao et al., 2023).

040 To achieve this, previous work has introduced numerous effective representation schemes in con-
041 trastive learning (Liu et al., 2023c), temporal prediction (Machado et al., 2023), and data augmen-
042 tation (Liu et al., 2023b). However, most existing contrastive and temporal prediction methods are
043 limited to learning vague classifications of structural features (Guo et al., 2023). Though they may
044 achieve fast convergence in specific tasks, they struggle with fine-grained feature control (Gao et al.,
045 2022). Regarding data augmentation-based methods, prior research has not yet clarified which ef-
046 fective features are associated with different transformations (Ma et al., 2024), and some setups face
047 difficulties in handling tasks with large action spaces and complex folded regions. Most importantly,
048 the above methods tend to represent all observable dynamics elements, limited by the task-agnostic
049 representation learning (Yuan et al., 2022; Zhang et al., 2021). As a result, these methods remain
050 inadequate for learning tasks with complex dynamics.

051 In contrast, representation learning built on bisimulation metrics (Ferns et al., 2004; 2011) has fun-
052 damentally shown promise in accurately extracting task-relevant information (Liao et al., 2023).
053 Distinct from the aforementioned methods, they extract equivalent task-relevant features by the be-
havioral similarity metric between states in terms of rewards and dynamics models, i.e., transition

distribution probability (Ferns et al., 2011), which has attracted much attention for their ability to eliminate all task-irrelevant information (Castro, 2020). Subsequently, related work focuses on overcoming its dynamics accuracy problem, e.g., π -bisimulation metric (Castro, 2020), and introducing additional elements or reward variance to enhance the robustness of the metric, e.g., PSE (Agarwal et al., 2021) and RAP (Chen & Pan, 2022), making it potentially applicable to large-scale tasks. Nevertheless, bisimulation metric-induced representation learning still suffers from information loss and even collapse problems in sparse reward settings (Liao et al., 2023; Zang et al., 2022). This is because, on the one hand, the idealized metric computations with reward difference significantly deviate from practical distances, which potentially leads to approximation bias and inaccurate behavioral similarity measurement (Zang et al., 2022; Castro et al., 2021); On the other hand, sparse or zero reward signals can cause bisimulation metrics to converge to an intractable zero-fixed point, resulting in representation collapse (Liao et al., 2023).

To tackle these issues, we first introduce a weak bisimulation metric, which excludes the unstable reward differences and instead relaxes the strict bisimulation metric with a trainable Gaussian distribution. Concretely, the weak bisimulation metric fine-tunes the metric distance by using the Gaussian noise associated with state transitions, which creates a flexible information margin for the optimization process, effectively avoiding the potential zero-distance representation between states, i.e., the representation collapse problem directly caused by sparse reward differences (Liao et al., 2023). Besides, since the trainable Gaussian distribution shares the same distribution dimensionality as the transition model in computations, the weak metric can potentially avoid inconsistent computations and further approximation bias within traditional metrics caused by strict assumptions (Zang et al., 2022). Although the metric adopts conservative settings, we theoretically demonstrate that it retains certain favorable properties. In further implementations, to strengthen the metric accordingly, we compute multi-step transition distribution differences on the metric to ensure the accuracy of the initial behavioral similarity by considering continuous similarity. Overall, our approach selectively performs effective relaxation or strengthening in specific aspects, and thus we term it scalable representation learning (SRL).

Finally, we conduct extensive experiments on challenging tasks with sparse rewards, i.e., the DeepMind Control, MetaWorld, and Adroit with large action spaces. Notably, most of these tasks feature sparse rewards, meaning they receive tiny rewards before successfully completing a task (Xu et al., 2024). The experimental results demonstrate that SRL significantly outperforms recent various state-of-the-art baselines across a massive number of complex tasks, as highlighted in the best scores shown in Figure 1. Additionally, ablation studies and visualization experiments (available in Appendix D.1 and Appendix D.2) strongly validate the effectiveness of the approach’s components in improving representation and policy performance.

The primary contributions of this work are as follows: (i) We propose a weak bisimulation metric with relaxed properties to address the potential representation instability in bisimulation metrics under sparse reward settings; (ii) Within this metric, we consider continuous transition distribution similarities to strengthen the initial behavior measurement, and then propose a scalable representation learning approach; (iii) We empirically demonstrate that SRL significantly outperforms state-of-the-art baselines on various tasks with sparse rewards, effectively extending the inherent advantages of bisimulation metric-based representations to a wider range of sparse reward scenarios.

2 RELATED WORK

DRL with vision as input aims to learn a policy directly from pixel observations (e.g., RGB images), which typically requires increasingly powerful feature representation abilities as the problem scales up (Ze et al., 2023; Nath et al., 2023; Kaufmann et al., 2023; Wang et al., 2023). In earlier work within the Atari 2600 gaming domain, to alleviate the limited representational capacity of end-to-end convolutional encoders, most studies converted RGB images to grayscale (Mnih et al., 2015).

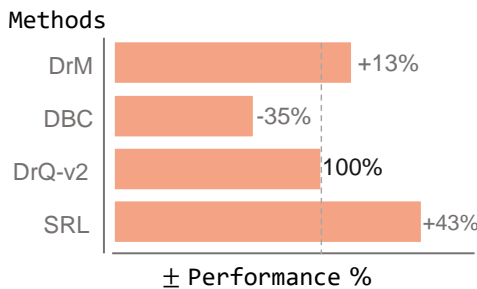


Figure 1: Comprehensive score performance of SRL and baselines compared to DrQ-v2 on DeepMind Control, MetaWorld, and Adroit.

As application scope expanded, recent work has adopted stacked RGB images as input to retain richer detail features (Yarats et al., 2021a; Yuan et al., 2023), but existing representation abilities are struggling to handle these complex and unstructured elements. To address this issue, although self-attention networks (Baee et al., 2021) and Transformers (Parisotto et al., 2020) were introduced early on to enhance feature extraction, Laskin et al. (2020a) demonstrated that these end-to-end optimization methods, sharing DRL gradients, often fail to achieve strong representation performance. As a result, recent work has increasingly focused on constructing effective self-supervised representation losses (Li et al., 2022; Yu et al., 2022), often referred to as auxiliary learning tasks. These approaches typically employ contrastive learning with data augmentation (Liu et al., 2021), latent reconstruction (Yu et al., 2022; Zhou et al., 2024), variational autoencoders (Liu et al., 2022), or the methods based on task elements (e.g., rewards), such as bisimulation metrics (Pavse & Hanna, 2024), reward prediction (Zhou et al., 2023), and state prediction (Fujimoto et al., 2024) to achieve more powerful representations through independent optimization losses.

Previous studies have shown that data augmentation, e.g., rotation, random cropping, random masking, and CycAug (Laskin et al., 2020b) can enhance representation learning algorithms' ability to understand and extract dynamics features (Hansen et al., 2021b; Yarats et al., 2021a). Typically, some research has proposed contrastive learning with data augmentation, where maximizing mutual information between positives and anchors (Oord et al., 2018) enhances consistency across different augmented versions. Nevertheless, Zhang et al. (2021) have pointed out that these methods are often constrained by task-agnostic learning. In other words, due to the randomness of augmentations, these approaches tend to extract all possible dynamics features from observations rather than focus on task-relevant ones (Zhang et al., 2021). To tackle this, some preliminary solutions have been proposed, which introduce actions (Hansen et al., 2021a) or rewards (Yang et al., 2022) to further constrain the dynamics feature set derived from data augmentation, resulting in decision vectors that exclude task-irrelevant features. Although these methods have shown some potential, they tend to underperform in practice, particularly in sparse reward environments.

Recently, the metric-based representation shows how to leverage task-related elements (e.g., rewards) to effectively infer equivalent task information from pixel observations (Liu et al., 2023a). Compared to methods like data augmentation, their key advantage lies in the theoretically task-relevant nature of the extracted features (Zang et al., 2024), such as the bisimulation metric-based approach DBC (Zhang et al., 2021). Specifically, bisimulation metric-based representation learning leverages bisimulation theory, exploiting rewards and transition distribution differences to infer equivalent task information from observations (Castro, 2020). However, numerous studies have shown that rigidly applying the bisimulation is not ideal (Chen & Pan, 2022; Castro et al., 2021), facing two major pitfalls: (i) It is difficult to overcome the computational complexity caused by model inaccuracy (Castro, 2020); (ii) The idealized metric computations with sparse-reward difference significantly deviate from practical distances (Liao et al., 2023). For the former, the π -bisimulation metric (Castro, 2020) mitigates this issue by considering state similarity under a specific policy. For the latter, while some works suggest relaxing the reward differences within bisimulation by incorporating learned reward variance (Chen & Pan, 2022), successfully applying bisimulation metrics to complex tasks with sparse rewards remains challenging (Liao et al., 2023). Hence, this work seeks to develop a relaxed bisimulation metric to adapt to such complex settings.

3 PRELIMINARIES

We start with the underlying assumptions of reinforcement learning (RL) and the notations. Following this, we review the bisimulation metrics used for representation learning, along with the practical optimization challenges.

3.1 REINFORCEMENT LEARNING

The interactive environment can be modeled as an infinite-horizon Markov Decision Process (MDP), defined by the tuple $\mathcal{M} = (\mathcal{S}, \mathcal{A}, \mathcal{P}, r, \gamma)$, where \mathcal{S} represents the state space, \mathcal{A} is the continuous action space, $\mathcal{P}(s_{t+1} | s_t, a_t) : \mathcal{S} \times \mathcal{A} \times \mathcal{S} \rightarrow [0, 1]$ defines the transition distribution that captures the probability from state s_t to state s_{t+1} with action a_t , $r : \mathcal{S} \times \mathcal{A} \rightarrow \mathbb{R}^1$ denotes the reward function, and $\gamma \in [0, 1]$ is the discount factor. As the image frame exhibits partial observability, we define the state s_t by stacking consecutive image frames. In the scope of representation learning for DRL, a parameterized state encoder $\phi_\omega : \mathcal{S} \rightarrow \mathbb{R}^n$ that maps a high-dimensional state to a low-dimensional

vector is learned. Then, the agent’s goal is to learn a good encoder and a policy $a_t \sim \pi(\phi_\omega(s_t))$ that maximizes the future cumulative discounted reward $\mathbb{E}_{\mathcal{P}, \pi}[\sum_{t=0}^{\infty} \gamma^t r(\phi_\omega(s_t), a_t)]$.

3.2 BISIMULATION METRIC

Bisimulation Relation(Givan et al., 2003) (formalized in Appendix B.1) is used to describe the behavioral similarity between abstract states, which is defined as if the rewards they obtain and the probability of the next transition distribution are equal, then they are considered to be behaviorally equivalent(Yarats et al., 2021a). To soften the Bisimulation Relation in the continuous state space (Ferns et al., 2011), past work defines the following pseudo-metric $d : \mathcal{S} \times \mathcal{S} \rightarrow \mathbb{R}^1$ to measure the similarity distance between states.

Theorem 3.1 (π -bisimulation metric (Castro, 2020)). *Let $d \in \mathbb{M}$ be a pseudometric on \mathbb{M} set over space \mathcal{S} . A pseudometric transformation function $\mathcal{F}_B^\pi : \mathbb{M} \rightarrow \mathbb{M}$, is defined as,*

$$\mathcal{F}_B^\pi(d)(s_i, s_j) = \left| \mathbb{E}_{a_i \sim \pi} r_{s_i}^{a_i} - \mathbb{E}_{a_j \sim \pi} r_{s_j}^{a_j} \right| + \gamma \mathcal{W}_1(d) \left(\mathcal{P}_{s_i}^\pi, \mathcal{P}_{s_j}^\pi \right) \quad (1)$$

Where transition model $\mathcal{P}_{s_i}^\pi = \mathbb{E}_{a \sim \pi(s_i)} \mathcal{P}_{s_i}^a$ and \mathcal{W}_1 is the 1-Wasserstein distance. \mathcal{F}_B^π has a least fixed point d_B^π and d_B^π is a π -bisimulation metric.

Theorem 3.2 (Value difference bound (Castro, 2020)). *Given any state pair $s_i, s_j \in \mathcal{S}$, and policy π , we have:*

$$|V^\pi(s_i) - V^\pi(s_j)| \leq d_B^\pi(s_i, s_j) \quad (2)$$

The theorem shows that the value function difference between state pairs is bounded by d_B^π , which will be used to compare the value difference bound of the weak bisimulation metric.

A zero bisimulation metric value between states indicates that they exhibit similar behavior and state values, yet metric-based representation learning does not aim to find perfectly similar states. Instead, the metric is employed to regularize the encoding distance $\|\phi_\omega(s_i) - \phi_\omega(s_j)\|_2$, so that the pixel states can be clustered to the same distance under latent space as the metric $d_B^\pi(s_i, s_j)$. Typically, the optimization of the bisimulation metric-based representation can be defined as,

$$\mathcal{L}(\phi_\omega) := \mathbb{E} \left[\left(\|\phi_\omega(s_i) - \phi_\omega(s_j)\|_2 - \left| \mathbb{E}_{a_i \sim \pi} r_{s_i}^{a_i} - \mathbb{E}_{a_j \sim \pi} r_{s_j}^{a_j} \right| - \gamma \mathcal{W}_1(d) \left(\mathcal{P}_{s_i}^\pi, \mathcal{P}_{s_j}^\pi \right) \right)^2 \right] \quad (3)$$

Ideally, minimizing $\mathcal{L}(\phi_\omega)$ loss be able to make ϕ_ω derive task-relevant features in each state and thereby learn the state representations guaranteed by bisimulation metrics. Nevertheless, strict assumptions make optimization challenging. In light of this, Zhang et al. (2021) require a stringent assumption that the states follow a Gaussian distribution, which makes it possible to calculate the closed-form Wasserstein distance with the Euclidean distance, but this is inconsistent with the L_1 distance on the reward, resulting in inaccurate bisimulation (Zang et al., 2022). On the other hand, strict bisimulation metrics built on rewards are naturally limited to sparse reward settings, which easily leads to representation collapse (Liao et al., 2023). In this paper, We attempt to improve the strict bisimulation metric and seek a reasonably scalable metric.

4 METHODOLOGY

In this section, we first investigate the weaknesses of prior bisimulation metric-based representations in terms of strict assumptions and sparse rewards, as well as the coupling factors that lead to the weaknesses, and then introduce a relaxed bisimulation metric. Then, to strengthen the weak metric accordingly, we implement a strengthened representation learning loss that can more strictly and accurately compute the dynamics transition difference. With these two steps, we finally present a scalable representation learning approach that is particularly suitable for sparse reward settings.

4.1 PROBLEMS OF BISIMULATION METRICS

Following the work of Castro (2020), we consider the policy-dependent (on-policy) π -bisimulation metric d^π to optimize the encoder ϕ_ω with parameter ω , where d^π can be selected from existing π -bisimulation-based d_B^π (Zhang et al., 2021), MICO(Castro et al., 2021), or RAP (Chen & Pan, 2022).

$$\phi^* = \arg \max_{\phi \in \Phi} \mathbb{E} \left[(\|\phi_\omega(s_i) - \phi_\omega(s_j)\|_2 - d^\pi(s_i, s_j))^2 \right] \quad (4)$$

In optional d^π , since Wasserstein distance is powerful to calculate the distributions' distance, it is often used to calculate internal state transition distribution difference $\mathcal{W}_1(d^\pi)(\mathcal{P}_{s_i}^\pi, \mathcal{P}_{s_j}^\pi)$. However, for large-scale tasks with continuous state space, it becomes impractical due to the need to enumerate all possible states. Thus, Zhang et al. (2021) require the strict assumption that the state distribution is a Gaussian, so that the closed-form Wasserstein distance can be calculated with the Euclidean distance in the latent space, which alleviates the computational complexity. However, there is an inconsistency (which can also be understood as a “dimensionality difference”) between the L_1 distance on rewards and the Euclidean distance, resulting in approximation deviation and further informative degradation (Zang et al., 2022). Although Castro et al. (2021) developed the MICo distance to maintain the consistency of the distance property, this distance that violates the “zero self-distance (Zang et al., 2022)” property may cause the representations to fail. Ultimately, this inconsistency between the transition distribution difference and reward difference makes the above objective (Equation (4)) difficult to optimize.

Besides the problem, the representation performance upon strict bisimulation metrics is unstable when facing sparse reward settings.

Theorem 4.1 (Liao et al. (2023)). π -bisimulation metrics have an upper bound determined by their policy π : $\text{diam}(\mathcal{S}; d^\pi) = \sup_{s_i, s_j \in \mathcal{S}} d^\pi(s_i, s_j) \leq \frac{1}{1-\gamma} \sup_{s_i, s_j \in \mathcal{S}} |\mathbb{E}_{a_i \sim \pi} r_{s_i}^{a_i} - \mathbb{E}_{a_j \sim \pi} r_{s_j}^{a_j}|$.

The proof can be found in the work (Liao et al., 2023). Theorem 4.1 shows that for a specific transition (s_i, s_j) , if it yields zero reward signals, the equation $|\mathbb{E}_{a_i \sim \pi} r_{s_i}^{a_i} - \mathbb{E}_{a_j \sim \pi} r_{s_j}^{a_j}| = 0$, which may cause a degenerate solution $\text{diam}(\mathcal{S}; d^\pi) = 0$. Deeply, this indicates that the latent distance between the states converges to a fixed zero, meaning that a collapsed encoder has been learned. For simple dense reward settings, the above problem is more likely to occur in the early training stage, because the initial policy may perform poorly everywhere. Still, from a long-term perspective, the π -bisimulation metrics will be gradually improved and become an advantage. But seriously, when in sparse reward settings, the reward collected by the policy may be zero everywhere, which may lead to constant representation collapse. Although part of the encoder's training gradients is backpropagated from Temporal-Difference loss in the Critic (Yarats et al., 2021b), this problem will still seriously interfere with the training of ϕ_ω .

4.2 WEAK BISIMULATION METRIC

We can easily conclude that the internal inconsistency problem of strict bisimulation metrics and the limitation of sparse rewards are actually coupled with the reward signal of the environment. In other words, the reward signal is a fundamental factor that causes the potential performance failure of the metrics. To comprehensively solve the above problems, we first introduce the following weak bisimulation metric to relax typical metrics.

Definition 4.2 (weak bisimulation metric). Let \mathbb{M} be the set of all pseudometrics on space \mathcal{S} . A pseudometric transformation function $\mathcal{F}_W^\pi : \mathbb{M} \rightarrow \mathbb{M}$, is defined as,

$$\mathcal{F}_W^\pi(d)(s_i, s_j) = \epsilon(s_i, s_j) - \gamma \mathcal{W}_1(d)(\mathcal{P}_{s_i}^\pi, \mathcal{P}_{s_j}^\pi) \quad (5)$$

where $\epsilon(s_i, s_j) \sim \mathcal{N}(\mu_c, f_{Var})$ with a constant μ_c and a nonlinear function $f_{Var}(s_i, s_j; \theta)$ as mean and variance respectively.

As shown in Definition 4.2, we define the weak bisimulation metric as consisting of the Wasserstein distance of state transition distributions and the parameterized Gaussian distribution $\epsilon(s_i, s_j)$, without the reward difference term.

We emphasize that this is not a semplice combination as it has the following considerations. First, since the reward signal itself is very small under sparse rewards, its contribution to similarity measurements is also weak in a sense. For relaxation reasons, we abandon the consideration of the $|\mathbb{E}_{a_i \sim \pi} r_{s_i}^{a_i} - \mathbb{E}_{a_j \sim \pi} r_{s_j}^{a_j}|$ in Equation (4) and instead introduce a trainable Gaussian distribution $\epsilon(s_i, s_j)$. Specifically, the mean $\mu_{c,(>0)}$ of $\epsilon(s_i, s_j)$ is a tiny constant set according to the sparse reward difference (see Appendix A.2 for details), which aims to potentially provide a non-zero metric to the worst-case $d^\pi(s_i, s_j)$, thereby preventing the degenerate solution $\text{diam}(\mathcal{S}; d^\pi) = 0$ caused by zero reward. In addition, since the variance of $\epsilon(s_i, s_j)$ is determined by the trainable function f_{Var} , this also allows the metric to be fine-tuned according to the current transition (s_i, s_j) . Finally, we embed the Gaussian distribution $\epsilon(s_i, s_j)$ into a computational dimensionality consistent with

270 the transition distribution, potentially avoiding the previous inconsistent computational problem be-
 271 tween the L_1 reward and the Wasserstein distance. This alignment ensures that the overall objective
 272 is optimized in the correct approximation direction.

273 We theoretically analyze some corresponding properties of the weak bisimulation metric below.
 274

275 **Lemma 4.3** (weak bisimulation metric). *The weak-bisimulation metric is a contraction mapping
 276 w.r.t the L^∞ norm on $\mathbb{R}^{\mathcal{S} \times \mathcal{S}}$, and there exists a fixed-point d_W^π for \mathcal{F}_W^π .*

277 The proof is available in Appendix A.1. This theory shows that the weak bisimulation metric can
 278 converge to a fixed point with iterative learning for any state pairs.
 279

280 **Theorem 4.4** (Value difference bound). *Given states s_i and s_j , and a policy π , we have,*
 281

$$|V^\pi(s_i) - V^\pi(s_j)| \leq d_W^\pi(s_i, s_j) \quad (6)$$

283 The proof can be found in Appendix A.2. Theorem 4.4 demonstrates that the difference of the state
 284 value function between any state pair is bounded by the weak bisimulation metric $d_W^\pi(s_i, s_j)$.
 285

286 **Theorem 4.5** (relaxed value difference bound). *Given states s_i and s_j , and a policy π , we have,*
 287

$$d_B^\pi(s_i, s_j) \leq d_W^\pi(s_i, s_j) \quad (7)$$

288 The proof is provided in Appendix A.2, which shows that $d_W^\pi(s_i, s_j)$ can achieve the difference
 289 upper bound of relaxing the original π -bisimulation metric $d_B^\pi(s_i, s_j)$. It is worth noting that, al-
 290 though it might reduce the correlation between the learned representation and the value function
 291 and further introduce redundant information (Chen & Pan, 2022), its advantages could outweigh the
 292 drawbacks due to the targeted relaxation for the intractable reward difference term. Specifically, in
 293 sparse reward settings, the reward term not only contributes minimally but also risks disrupting the
 294 learned representation. For this reason, we conservatively replace the reward term with a Gaussian
 295 distribution and set its mean $\mu_c \geq |\mathbb{E}_{a_i \sim \pi} r_{s_i}^{a_i} - \mathbb{E}_{a_j \sim \pi} r_{s_j}^{a_j}|$ (the reward term is typically minimal,
 296 details in Appendix A.2), aiming to release only the uncontrollable information measured by the
 297 reward difference. Although our metric may introduce certain redundant information, it is at least
 298 improvable rather than deadly. Therefore, we still consider this targeted relaxation as a beneficial
 299 strategy, with its existing shortcomings set to be addressed in future improvements.
 300

4.3 THE SCALABLE REPRESENTATION LEARNING

301 This section analyzes the optimization objective grounded in weak bisimulation and further consid-
 302 ers strengthening the objective by accumulating state transition distribution differences accordingly.
 303 These two steps ultimately lead to a scalable representation learning loss.
 304

305 First, according to the weak bisimulation metric (Equation (5)) in Definition 4.2, we set the learning
 306 target as:
 307

$$\mathcal{T}(s_i, s_j; \bar{\omega}, \theta) = \epsilon_\theta(\bar{z}_i, \bar{z}_j) + \mathbb{E}_{\substack{s \sim \hat{\mathcal{P}} \\ a \sim \pi}} \gamma \mathcal{W}_1(d_W^\pi) \left(\hat{\mathcal{P}}_\psi^\pi(\bar{z}_i, a), \hat{\mathcal{P}}_\psi^\pi(\bar{z}_j, a) \right) \quad (8)$$

309 where $z = \phi_\omega(s)$ represents the latent state, \bar{z} is frozen with gradient-free parameter $\bar{\omega}$, and ψ
 310 denotes the parameter of the learned dynamics model $\hat{\mathcal{P}}$. The variance of $\epsilon_\theta(\bar{z}_i, \bar{z}_j)$ draws from
 311 the network $f_{Var}(\bar{z}_i, \bar{z}_j; \theta)$ with parameters θ . Notably, we train the distribution function ϵ_θ by
 312 sampling $\tilde{\epsilon} \sim \mathcal{N}(\mu_c, f_{Var})$. To ensure its differentiability, we need to reparameterize $\tilde{\epsilon}$ by, $\tilde{\epsilon} =$
 313 $\mu_c + \sigma_1 f_{Var}(\bar{z}_i, \bar{z}_j; \theta)$, where $\sigma_1 \sim \mathcal{N}(0, 1)$.
 314

315 Therefore, we give the preliminary representation learning loss based on the target,
 316

$$\mathcal{L}^{weak}(\phi_\omega, \theta) = \mathbb{E}_{\mathcal{D}} [\|\phi_\omega(s_i) - \phi_\omega(s_j)\|_2 - \mathcal{T}(s_i, s_j; \bar{\omega}, \theta)] \quad (9)$$

317 Although the above objective is effective, it is not enough. As aforementioned, Theorem 4.5 has
 318 shown that our metric d_W^π has a looser value difference bound than the vanilla bisimulation metric,
 319 resulting in introducing potentially redundant information in addition to the superiority of avoiding
 320 unstable representations.
 321

322 To improve this, we try to strengthen the transition distribution difference of the weak bisimulation
 323 metric. Specifically, we further come up with the cumulative $\mathcal{W}_1(\hat{\mathcal{P}}_z^\pi, \hat{\mathcal{P}}_z^\pi)$ distance of the subse-
 324 quent T -step transition distributions started with (s_i, s_j) . The purpose is to make its subsequent

distributions as consistent as possible, thereby improving the distance's accuracy of the initial transition distribution. To balance the accuracy of the parameterized dynamics model $\hat{\mathcal{P}}$, T is actually set to 2, see Section 5.3 for detailed analysis. Notably, since the transition distribution differences are executed over the 50-dimensional latent state, the resulting computational overhead is negligible. As a result, we define the following scalable representation learning loss,

$$\mathcal{L}^{weak}(\phi_\omega, \theta) = \mathbb{E}_{\mathcal{D}} \left[\|\phi_\omega(s_i) - \phi_\omega(s_j)\|_2 - \mathcal{T}^{(T)}(s_i, s_j; \bar{\omega}; \theta) \right]^2 \quad (10)$$

with the learning target,

$$\mathcal{T}^{(T)}(s_i, s_j; \bar{\omega}, \theta) = \epsilon_\theta(\bar{z}_i, \bar{z}_j) + \sum_{t=1}^{T=2} \mathbb{E}_{\substack{s \sim \hat{\mathcal{P}} \\ a \sim \pi}} \left[\gamma^t \mathcal{W}_1 \left(\hat{\mathcal{P}}_\psi^\pi(\bar{z}_i^{(t)}, a^{(t)}), \hat{\mathcal{P}}_\psi^\pi(\bar{z}_j^{(t)}, a^{(t)}) \right) \right] \quad (11)$$

Specifically, due to sparse rewards or zero rewards, methods based on bisimulation metrics are prone to mistakenly infer that two states are bisimilarity based on the one-step transition difference, which causes the encoder to converge prematurely. In fact, a similar problem was also pointed out in the work of Kemertas & Aumentado-Armstrong (2021), which showed that trajectory information may be needed to assist bisimulation metrics under sparse rewards. Given this, we propose the above operation on the weak metric to ensure the consistency of continuous transitions, i.e., latent trajectories, thereby improving the accuracy of current behavior similarity and the extraction of further task-relevant features.

In summary, we propose the above scalable representation learning loss (Equation (10)), where the scalability lies in the purposeful relaxation of the original bisimulation metric and the strict operation of the transfer distribution differentiation, as well as their potential mutual constraints.

4.4 OVERALL ARCHITECTURE

We extend the scalable representation learning loss $\mathcal{L}^{weak}(\phi_\omega, \theta)$ built on the weak bisimulation metric to the visual RL algorithm DrQ-v2 (Yarats et al., 2021b), as shown in Figure 2. The encoder ϕ_ω is the core optimization component in the architecture, and its training gradients are propagated by the scalable representation learning loss and Temporal-Difference loss (Lee & He, 2019). Additionally, during the optimization of $\mathcal{L}^{weak}(\phi_\omega, \theta)$, a dynamics model $\hat{\mathcal{P}}_\psi^\pi$ needs to be trained synchronously. Finally, the primary loss denotes $\mathcal{L}^{weak} + \mathcal{L}^\pi + \mathcal{L}^Q$, where $\mathcal{L}^\pi + \mathcal{L}^Q$ is the internal Actor-Critic loss (available in Appendix C.1) of DrQ-v2. The detailed algorithm can be found in Appendix C.3.

5 EXPERIMENTS

This section aims to verify SRL's representation ability and policy performance in visual tasks with sparse rewards. We extensively compare SRL with state-of-the-art baselines across three visual environments, ranging from classic physics control to robotic manipulation: DeepMind Control Suite (DMControl) (Tassa et al., 2018), MetaWorld (Yu et al., 2020), and Adroit (Rajeswaran et al., 2017) (depicted in Figure 3). It is worth noting that most of these task settings are highly challenging, featuring rich visual details or large action spaces. Furthermore, the agent can only obtain a larger reward by continuous trial and error until it successfully completes a task.

Baselines. We compare against DrQ-v2 (Yarats et al., 2021b), DBC (Zhang et al., 2021), and DrM (Xu et al., 2024) DRL baselines that focus on representation ability or sparse-reward settings. DrQ-v2 is a powerful method based on data augmentation, achieving state-of-the-art sample efficiency on the DMControl benchmark. Of its lesser hyperparameters and stable performance, DrQ-v2 is commonly used as the foundational framework for various DRL methods (Xu et al., 2024). DBC is a bisimulation metric-based representation learning method, where the metric calculates the reward

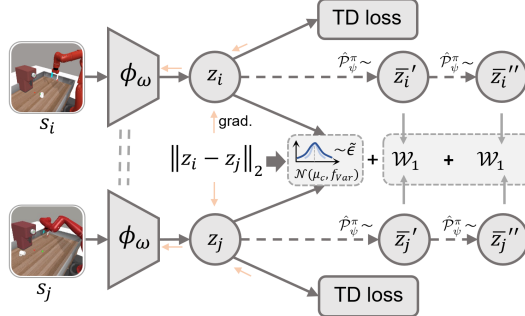


Figure 2: **Overall Architecture.** We use the architecture to describe scalable representation learning for deep reinforcement learning.

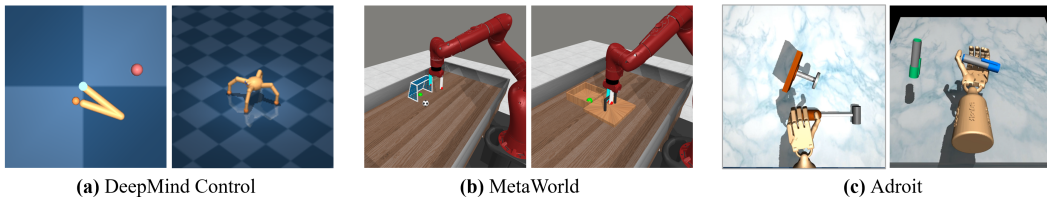


Figure 3: Illustration of partial tasks in DMControl, MetaWorld, and Adroit.

and transition distribution difference according to strict assumptions. It shows the superior ability to extract task features in the Distracting DMControl benchmark (Stone et al., 2021). DrM, a state-of-the-art method, proposes a dormant ratio minimization to promote representation and exploration under sparse rewards, achieving the best performance in various environments such as MetaWorld.

Settings. We employ the same encoder and hyperparameter settings in the involved methods. Specifically, the encoder consists of a 4-layer convolution network and a 2-layer full connection network with 1024 hidden neurons, which maps three stacked RGB observation images with size $9 \times 84 \times 84$ to a 50-dimensional feature vector for policy learning. Moreover, we utilize the Adam optimizer (Kingma, 2014) with a batch size of 256 and a learning rate of $1e^{-4}$. Distinct from the previous replay buffer with a size of $1e^6$, we set it to the challenging size of $2e^5$. The full hyperparameters are available in Appendix C.2.

5.1 DMCONTROL EXPERIMENTS

DMControl Suite. DMControl Suite is a widely used benchmark for DRL algorithms, which provides physics control tasks in different difficulties and supports rendering third-person pixel observations as training input (Tassa et al., 2018). We choose complex `walker_walk`, `walker_run`, `reacher_hard` and `quadruped_run` tasks with sparse rewards properties to evaluate our method. The illustrations of DMControl tasks can be seen in Fig. 3. (a).

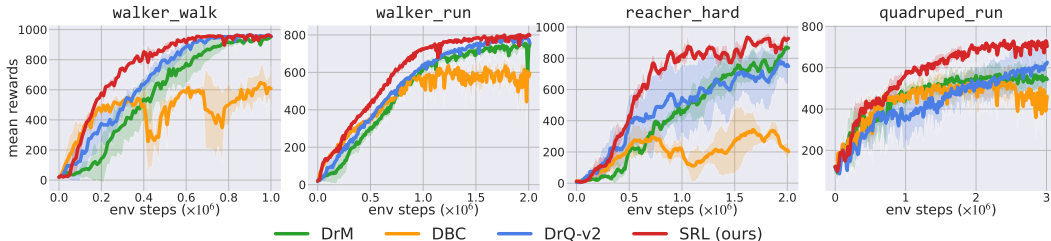


Figure 4: Experimental results on 4 complex tasks in DMControl. Each curve is averaged over three seeds with one standard deviation shaded in the default setting. For each seed, the mean episode reward is evaluated every 5,000 training steps, averaging over 10 episodes.

DMControl results. We show the evaluation curves of the SRL method compared with baselines on DMControl in Figure 4. From the upward trend and the convergence range of curves, our method has achieved the best performance in the four tasks, both in terms of convergence speed and best mean episodic rewards. Specifically, with the policy and value network modules kept consistent, the SRL equipped with the weak bisimulation representation learning (red line) significantly outperforms the latest DrM (green line), showing a substantial improvement in the DMControl domain. Notably, compared to the DBC method (yellow line), which is also grounded in bisimulation representation, SRL learns a robust and efficient policy for some challenging tasks, such as the `reacher_hard` task. Overall, we preliminarily conclude that the relaxed weak bisimulation metric-based representation enhances the encoder’s ability to extract task-relevant features, providing high-quality latent states for policy learning.

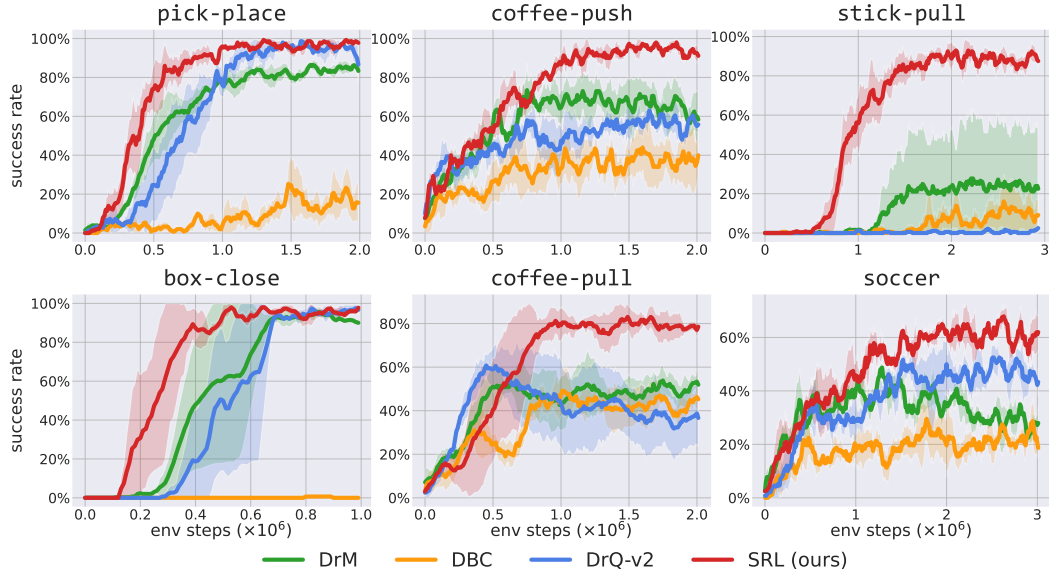
Table 1 records the comparison results on the best mean episode reward. The result shows that SRL has achieved a significant improvement in the best reward compared to baselines. In comparison, the sibling method, i.e., DBC almost achieved the lowest score in the difficult DMControl task, especially the worst performance in `reacher_hard`.

Table 1: Comparison results of the best mean episode reward on complex DMControl tasks.

Methods	walker_w	walker_r	reacher_h	quad_r
DrQ	944.5 \pm 24.6	755.2 \pm 33.2	871.8 \pm 30.1	570.2 \pm 76.9
DBC	648.4 \pm 105.6	634.7 \pm 38.3	342.9 \pm 109.5	530.9 \pm 83.7
DrQ-v2	963.5 \pm 11.4	789.6 \pm 19.9	784.0 \pm 104.6	626.4 \pm 120.1
SRL (ours)	965.9\pm2.0	803.2\pm10.2	935.7\pm12.1	732.4\pm9.9

432 5.2 ROBOTIC MANIPULATION EXPERIMENTS
 433

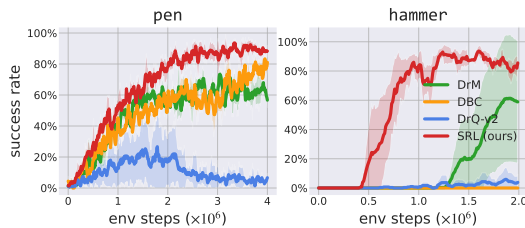
434 **Robotic Manipulation tasks.** The experiments are evaluated on MetaWorld and Adroit environments
 435 with sparse-reward settings, where MetaWorld contains various mechanical arm tasks (e.g.,
 436 coffee-push) and Adroit aims to control a dexterous hand with a large action space to achieve
 437 various delicate tasks. The illustrations of MetaWorld and Adroit tasks can be seen in Figure 3 (b)
 438 and Figure 3 (c). We emphasize that the field of robotic manipulations is extremely challenging
 439 for visual DRL algorithms without real state information. On the one hand, the kinematic struc-
 440 ture characteristics of these tasks are extremely complex, requiring the representation algorithm to
 441 fundamentally understand the dynamics knowledge and extract the implicit task-relevant features;
 442 On the other hand, due to the obvious sparse reward nature, it requires the agent to have long-term
 443 planning abilities and remarkable representation performance under sparse rewards.
 444



451 Figure 5: Experimental results on 6 complex tasks with sparse rewards in MetaWorld. Each curve is
 452 averaged over three seeds with one standard deviation shaded in the default setting. For each seed,
 453 the mean episode reward is evaluated every 5,000 training steps, averaging over 10 episodes.
 454

455 **MetaWorld results.** As depicted in Figure 5, we evaluate the performance of SRL against base-
 456 lines on 6 complex tasks with sparse rewards in MetaWorld. Following the experimental de-
 457 tails of the work (Xu et al., 2024), we use task success rate as the core comparison metric and
 458 train for 1–4 M ($1e^6$) environment steps based on the convergence of tasks. Overall, the SRL
 459 method achieves the highest success rate in all tasks and is significantly higher than the sub-
 460 optimal DrM method. For instance, in the stick-pull task, our method achieves an aver-
 461 age success rate of nearly 90%, while the baseline struggles to break 30%. In addition, com-
 462 bined with the reward curves in Figure 10 (in Appendix D.3), we can also observe that SRL
 463 can quickly obtain rewards and learn policies, and the learning is more stable. In contrast, al-
 464 though the DBC policy has rich task-related elements, it is difficult to obtain reward signals in
 465 most tasks, far below the SRL performance. This further empirically shows that, although the
 466 bisimulation metric can strictly guarantee that DBC with reward difference achieves equivalent
 467 task-relevant information, it is still unable to combine rewards to infer equivalent task features,
 468 yet even obtains a damaged representation space, resulting in inefficient policies in these tasks.
 469

470 **Adroit results.** To verify the visual represen-
 471 tation ability of SRL under extremely complex
 472 dynamics structures, we also evaluated it on the
 473 Pen and Hammer tasks in the Adroit environ-
 474 ment, as shown in Figure 6. Despite the po-
 475 tential blind spots or overlaps of observations
 476 rendered from a fixed-position third-person per-
 477 spective, experimental results show that our
 478



479 Figure 6: Experimental results on two Adroit tasks
 480 with sparse rewards over three seeds.
 481

method can still accelerate training and outperform state-of-the-art methods in these tasks. As for the baseline, we found that DrQ-v2 has difficulty using data augmentation to understand the features of the Adroit task with complex visual structures, which leads to ineffective policy learning. This is consistent with Zhang et al. (2021) and previous experimental results. In addition, although DrM is good at representation learning under sparse rewards, it is still difficult to surpass our method, especially in the hammer task.

In Table 2, we record the best mean success rate of SRL and baselines in MetaWorld and Adroit tasks. Our method has a success rate of more than 90% in most tasks and learns an effective policy. In addition, the overall variance of SRL is smaller than that of baselines, so the learned policy is more robust.

Table 2: Comparison results of the best mean success rate (%) on complex MetaWorld and Adroit tasks with sparse rewards.

Methods	pick-place	coffee-push	stick-pull	box-close	coffee-pull	soccer	pen	hammer
DrM	86.4±2.9	73.5±14.0	27.8±35.8	95.7±2.5	53.8±7.2	48.8±2.0	73.3±4.1	61.3±43.6
DBC	25.3±10.9	44.7±5.2	16.1±13.6	0.0±0.0	49.2±11.3	29.6±8.5	83.3±1.9	0.0±0.0
DrQ-v2	98.7±1.9	63.0±6.1	2.5±3.5	97.5±2.0	60.8±5.1	52.5±4.4	26.7±27.2	6.0±8.5
SRL (ours)	99.3±0.9	98.0±0.0	92.9±4.6	98.0±0.0	83.1±6.2	67.9±4.8	93.5±1.7	93.7±3.4

5.3 ABLATION STUDY

As depicted in Figure 7, to observe how the T -step transition distribution differences affect weak bisimulation metric-based representation learning, we execute the ablation study of SRL with the settings of step $T = \{1, 2, 3\}$ in several tasks. To better distinguish the convergence performance among policies, we record the score of 1/2 total training frames. From the figure, we can draw the following results: i) The performance of the SRL policies with $T = \{1, 2, 3\}$ settings all surpasses the DrQ-v2 ($T = 0$), which strongly demonstrates the effectiveness of the fundamental weak bisimulation metric; ii) For the specific $T = \{1, 2, 3\}$, the policies performance is $SRL_{T=2} > SRL_{T=1} > SRL_{T=3}$. In other words, cumulative multi-step transition distribution differences have the potential to improve the representation ability of weak bisimulation metric, but its performance tends to decay with the increase of the steps. We argue that the decay at $T = 3$ may be led by the accumulated deviation of the learned dynamics model $\hat{\mathcal{P}}_\psi$. For this reason, we set $T = 2$ to tighten the state similarity measure of the weak bisimulation metric in the scalable representation learning loss, achieving the best representation learning performance. Note again that since the transition differences are performed on the latent states, the computational overhead remains negligible.

6 CONCLUSION

In this paper, we propose a simple but efficient scalable representation learning approach (SRL) based on a new weak bisimulation metric in sparse reward settings. Overall, SRL alleviates the potential inefficient representations and limitations caused by strict bisimulation metrics under sparse reward settings by relaxing the reward difference term and strengthening the effectiveness of transition distribution differences. Additionally, we briefly analyze the favorable value difference bound and the convergence of the weak bisimulation metric. Extensive comparative experiments across complex tasks in the DMControl, MetaWorld, and Adroit environments verify the state-of-the-art performance of these simple settings. Finally, SRL extends the methods’ advantages built on the bisimulation concept, i.e., inherently good at extracting task-relevant information, to a wider range of sparse-reward task scenarios.

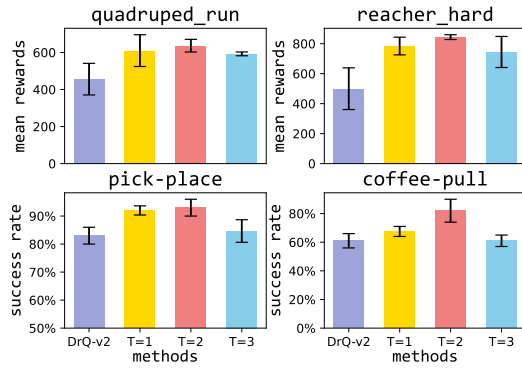


Figure 7: Ablation study in SRL. Each result is the average of three seeds, where the boundary represents the standard deviation. DrQ-v2 can be regarded as a degenerate version with $N = 0$.

We argue that the decay at $T = 3$ may be led by the accumulated deviation of the learned dynamics model $\hat{\mathcal{P}}_\psi$. For this reason, we set $T = 2$ to tighten the state similarity measure of the weak bisimulation metric in the scalable representation learning loss, achieving the best representation learning performance. Note again that since the transition differences are performed on the latent states, the computational overhead remains negligible.

540 REFERENCES
541

- 542 Rishabh Agarwal, Marlos C Machado, Pablo Samuel Castro, and Marc G Bellemare. Contrastive
543 behavioral similarity embeddings for generalization in reinforcement learning. *arXiv preprint*
544 *arXiv:2101.05265*, 2021.
- 545 Sonia Baee, Erfan Pakdamanian, Inki Kim, Lu Feng, Vicente Ordonez, and Laura Barnes. Medirl:
546 Predicting the visual attention of drivers via maximum entropy deep inverse reinforcement learn-
547 ing. In *Proceedings of the IEEE/CVF international conference on computer vision*, pp. 13178–
548 13188, 2021.
- 549 Gabriel Barth-Maron, Matthew W Hoffman, David Budden, Will Dabney, Dan Horgan, TB Dhruva,
550 Alistair Muldal, Nicolas Heess, and Timothy Lillicrap. Distributed distributional deterministic
551 policy gradients. In *International Conference on Learning Representations*, 2018.
- 552 Pablo Samuel Castro. Scalable methods for computing state similarity in deterministic markov
553 decision processes. In *Proceedings of the AAAI Conference on Artificial Intelligence*, volume 34,
554 pp. 10069–10076, 2020.
- 555 Pablo Samuel Castro, Tyler Kastner, Prakash Panangaden, and Mark Rowland. Mico: Improved
556 representations via sampling-based state similarity for markov decision processes. *Advances in*
557 *Neural Information Processing Systems*, 34:30113–30126, 2021.
- 558 Jianda Chen and Sinno Pan. Learning representations via a robust behavioral metric for deep re-
559 inforcement learning. *Advances in Neural Information Processing Systems*, 35:36654–36666,
560 2022.
- 561 Norm Ferns, Prakash Panangaden, and Doina Precup. Metrics for finite markov decision processes.
562 In *UAI*, volume 4, pp. 162–169, 2004.
- 563 Norm Ferns, Prakash Panangaden, and Doina Precup. Bisimulation metrics for continuous markov
564 decision processes. *SIAM Journal on Computing*, 40(6):1662–1714, 2011.
- 565 Scott Fujimoto, Wei-Di Chang, Edward Smith, Shixiang Shane Gu, Doina Precup, and David Meger.
566 For sale: State-action representation learning for deep reinforcement learning. *Advances in Neural*
567 *Information Processing Systems*, 36, 2024.
- 568 Junyu Gao, Mengyuan Chen, and Changsheng Xu. Fine-grained temporal contrastive learning for
569 weakly-supervised temporal action localization. In *Proceedings of the IEEE/CVF conference on*
570 *computer vision and pattern recognition*, pp. 19999–20009, 2022.
- 571 Robert Givan, Thomas Dean, and Matthew Greig. Equivalence notions and model minimization in
572 markov decision processes. *Artificial intelligence*, 147(1-2):163–223, 2003.
- 573 Qiushan Guo, Yizhou Yu, Yi Jiang, Jiannan Wu, Zehuan Yuan, and Ping Luo. Multi-level contrastive
574 learning for dense prediction task. *arXiv preprint arXiv:2304.02010*, 2023.
- 575 Nicklas Hansen, Rishabh Jangir, Guillem Alenyà Ribas, Pieter Abbeel, Alexei Efros A, Lerrel Pinto,
576 and Xiaolong Wang. Self-supervised policy adaptation during deployment. In *International*
577 *Conference on Learning Representations, ICLR 2021: Vienna, Austria, May 04 2021*, pp. 1–18.
578 OpenReview. net, 2021a.
- 579 Nicklas Hansen, Hao Su, and Xiaolong Wang. Stabilizing deep q-learning with convnets and vision
580 transformers under data augmentation. *Advances in neural information processing systems*, 34:
581 3680–3693, 2021b.
- 582 Elia Kaufmann, Leonard Bauersfeld, Antonio Loquercio, Matthias Müller, Vladlen Koltun, and
583 Davide Scaramuzza. Champion-level drone racing using deep reinforcement learning. *Nature*,
584 620(7976):982–987, 2023.
- 585 Mete Kemertas and Tristan Aumentado-Armstrong. Towards robust bisimulation metric learning.
586 *Advances in Neural Information Processing Systems*, 34:4764–4777, 2021.

- 594 Diederik P Kingma. Adam: A method for stochastic optimization. *arXiv preprint arXiv:1412.6980*,
 595 2014.
- 596
- 597 Vijay R Konda and John N Tsitsiklis. Actor-critic algorithms. In *Proceedings of the 12th International*
 598 *Conference on Neural Information Processing Systems*, pp. 1008–1014, 1999.
- 599 Michael Laskin, Aravind Srinivas, and Pieter Abbeel. Curl: Contrastive unsupervised representa-
 600 tions for reinforcement learning. In *International conference on machine learning*, pp. 5639–
 601 5650. PMLR, 2020a.
- 602
- 603 Misha Laskin, Kimin Lee, Adam Stooke, Lerrel Pinto, Pieter Abbeel, and Aravind Srinivas. Rein-
 604 forcement learning with augmented data. *Advances in neural information processing systems*, 33:
 605 19884–19895, 2020b.
- 606
- 607 Donghwan Lee and Niao He. Target-based temporal-difference learning. In *International Confer-*
 608 *ence on Machine Learning*, pp. 3713–3722. PMLR, 2019.
- 609
- 610 Xiang Li, Jinghuan Shang, Srijan Das, and Michael Ryoo. Does self-supervised learning really im-
 611 prove reinforcement learning from pixels? *Advances in Neural Information Processing Systems*,
 35:30865–30881, 2022.
- 612
- 613 Weijian Liao, Zongzhang Zhang, and Yang Yu. Policy-independent behavioral metric-based repre-
 614 sentation for deep reinforcement learning. In *Proceedings of the AAAI Conference on Artificial*
Intelligence, volume 37, pp. 8746–8754, 2023.
- 615
- 616 Fangchen Liu, Hao Liu, Aditya Grover, and Pieter Abbeel. Masked autoencoding for scalable and
 617 generalizable decision making. *Advances in Neural Information Processing Systems*, 35:12608–
 12618, 2022.
- 618
- 619 Guoqing Liu, Chuheng Zhang, Li Zhao, Tao Qin, Jinhua Zhu, Li Jian, Nenghai Yu, and Tie-Yan
 620 Liu. Return-based contrastive representation learning for reinforcement learning. In *International*
Conference on Learning Representations, 2021.
- 621
- 622 Qiyuan Liu, Qi Zhou, Rui Yang, and Jie Wang. Robust representation learning by clustering with
 623 bisimulation metrics for visual reinforcement learning with distractions. In *Proceedings of the*
624 AAAI Conference on Artificial Intelligence, volume 37, pp. 8843–8851, 2023a.
- 625
- 626 Siao Liu, Zhaoyu Chen, Yang Liu, Yuzheng Wang, Dingkang Yang, Zhile Zhao, Ziqing Zhou, Xie
 627 Yi, Wei Li, Wenqiang Zhang, et al. Improving generalization in visual reinforcement learning via
 628 conflict-aware gradient agreement augmentation. In *Proceedings of the IEEE/CVF International*
629 Conference on Computer Vision, pp. 23436–23446, 2023b.
- 630
- 631 Sicong Liu, Xi Sheryl Zhang, Yushuo Li, Yifan Zhang, and Jian Cheng. On the data-efficiency
 632 with contrastive image transformation in reinforcement learning. In *The Eleventh International*
Conference on Learning Representations, 2023c.
- 633
- 634 Guozheng Ma, Linrui Zhang, Haoyu Wang, Lu Li, Zilin Wang, Zhen Wang, Li Shen, Xueqian Wang,
 635 and Dacheng Tao. Learning better with less: effective augmentation for sample-efficient visual
 reinforcement learning. *Advances in Neural Information Processing Systems*, 36, 2024.
- 636
- 637 Marlos C Machado, Andre Barreto, Doina Precup, and Michael Bowling. Temporal abstraction in
 638 reinforcement learning with the successor representation. *Journal of Machine Learning Research*,
 24(80):1–69, 2023.
- 639
- 640 Volodymyr Mnih, Koray Kavukcuoglu, David Silver, Andrei A Rusu, Joel Veness, Marc G Belle-
 641 mare, Alex Graves, Martin Riedmiller, Andreas K Fidjeland, Georg Ostrovski, et al. Human-level
 642 control through deep reinforcement learning. *nature*, 518(7540):529–533, 2015.
- 643
- 644 Somjit Nath, Gopeshh Subbaraj, Khimya Khetarpal, and Samira Ebrahimi Kahou. Discovering
 645 object-centric generalized value functions from pixels. In *International Conference on Machine*
Learning, pp. 25755–25768. PMLR, 2023.
- 646
- 647 Aaron van den Oord, Yazhe Li, and Oriol Vinyals. Representation learning with contrastive predic-
 tive coding. *arXiv preprint arXiv:1807.03748*, 2018.

- 648 Emilio Parisotto, Francis Song, Jack Rae, Razvan Pascanu, Caglar Gulcehre, Siddhant Jayakumar,
 649 Max Jaderberg, Raphael Lopez Kaufman, Aidan Clark, Seb Noury, et al. Stabilizing transformers
 650 for reinforcement learning. In *International conference on machine learning*, pp. 7487–7498.
 651 PMLR, 2020.
- 652 Brahma Pavse and Josiah Hanna. State-action similarity-based representations for off-policy evalua-
 653 tion. *Advances in Neural Information Processing Systems*, 36, 2024.
- 654 Aravind Rajeswaran, Vikash Kumar, Abhishek Gupta, Giulia Vezzani, John Schulman, Emanuel
 655 Todorov, and Sergey Levine. Learning complex dexterous manipulation with deep reinforcement
 656 learning and demonstrations. *arXiv preprint arXiv:1709.10087*, 2017.
- 657 Austin Stone, Oscar Ramirez, Kurt Konolige, and Rico Jonschkowski. The distracting con-
 658 trol suite—a challenging benchmark for reinforcement learning from pixels. *arXiv preprint*
 659 *arXiv:2101.02722*, 2021.
- 660 Adam Stooke, Kimin Lee, Pieter Abbeel, and Michael Laskin. Decoupling representation learning
 661 from reinforcement learning. In *International conference on machine learning*, pp. 9870–9879.
 662 PMLR, 2021.
- 663 Yunhao Tang, Zhaohan Daniel Guo, Pierre Harvey Richemond, Bernardo Avila Pires, Yash Chan-
 664 dak, Rémi Munos, Mark Rowland, Mohammad Gheshlaghi Azar, Charline Le Lan, Clare Lyle,
 665 et al. Understanding self-predictive learning for reinforcement learning. In *International Confer-
 666 ence on Machine Learning*, pp. 33632–33656. PMLR, 2023.
- 667 Yuval Tassa, Yotam Doron, Alistair Muldal, Tom Erez, Yazhe Li, Diego de Las Casas, David Bud-
 668 den, Abbas Abdolmaleki, Josh Merel, Andrew Lefrancq, et al. Deepmind control suite. *arXiv*
 669 *preprint arXiv:1801.00690*, 2018.
- 670 Cédric Villani. *Topics in optimal transportation*, volume 58. American Mathematical Soc., 2021.
- 671 Shuo Wang, Zhihao Wu, Xiaobo Hu, Youfang Lin, and Kai Lv. Skill-based hierarchical reinfor-
 672 cements learning for target visual navigation. *IEEE Transactions on Multimedia*, 25:8920–8932,
 673 2023.
- 674 Yiming Wang, Ming Yang, Renzhi Dong, Binbin Sun, Furui Liu, et al. Efficient potential-based
 675 exploration in reinforcement learning using inverse dynamic bisimulation metric. *Advances in
 676 Neural Information Processing Systems*, 36, 2024.
- 677 Guowei Xu, Ruijie Zheng, Yongyuan Liang, Xiyao Wang, Zhecheng Yuan, Tianying Ji, Yu Luo,
 678 Xiaoyu Liu, Jiaxin Yuan, Pu Hua, et al. Drm: Mastering visual reinforcement learning through
 679 dormant ratio minimization. In *The Twelfth International Conference on Learning Representa-
 680 tions*, 2024.
- 681 Rui Yang, Jie Wang, Zijie Geng, Mingxuan Ye, Shuiwang Ji, Bin Li, and Feng Wu. Learning
 682 task-relevant representations for generalization via characteristic functions of reward sequence
 683 distributions. In *Proceedings of the 28th ACM SIGKDD Conference on Knowledge Discovery
 684 and Data Mining*, pp. 2242–2252, 2022.
- 685 Denis Yarats, Rob Fergus, and Ilya Kostrikov. Image augmentation is all you need: Regularizing
 686 deep reinforcement learning from pixels. In *9th International Conference on Learning Represen-
 687 tations*, 2021a.
- 688 Denis Yarats, Rob Fergus, Alessandro Lazaric, and Lerrel Pinto. Mastering visual continuous con-
 689 trol: Improved data-augmented reinforcement learning. In *International Conference on Learning
 690 Representations*, 2021b.
- 691 Tao Yu, Zhizheng Zhang, Cuiling Lan, Yan Lu, and Zhibo Chen. Mask-based latent reconstruc-
 692 tion for reinforcement learning. *Advances in Neural Information Processing Systems*, 35:25117–
 693 25131, 2022.
- 694 Tianhe Yu, Deirdre Quillen, Zhanpeng He, Ryan Julian, Karol Hausman, Chelsea Finn, and Sergey
 695 Levine. Meta-world: A benchmark and evaluation for multi-task and meta reinforcement learning.
 696 In *Conference on robot learning*, pp. 1094–1100. PMLR, 2020.

- 702 Zhecheng Yuan, Guozheng Ma, Yao Mu, Bo Xia, Bo Yuan, Xueqian Wang, Ping Luo, and Huazhe
 703 Xu. Don't touch what matters: Task-aware lipschitz data augmentation for visual reinforcement
 704 learning. *arXiv preprint arXiv:2202.09982*, 2022.
- 705 Zhecheng Yuan, Sizhe Yang, Pu Hua, Can Chang, Kaizhe Hu, and Huazhe Xu. Rl-vigen: a rein-
 706 force learning benchmark for visual generalization. In *Proceedings of the 37th International*
 707 *Conference on Neural Information Processing Systems*, pp. 6720–6747, 2023.
- 708 Hongyu Zang, Xin Li, and Mingzhong Wang. Simsr: Simple distance-based state representations
 709 for deep reinforcement learning. In *Proceedings of the AAAI Conference on Artificial Intelligence*,
 710 volume 36, pp. 8997–9005, 2022.
- 711 Hongyu Zang, Xin Li, Leiji Zhang, Yang Liu, Baigui Sun, Riashat Islam, Remi Tachet des Combes,
 712 and Romain Laroche. Understanding and addressing the pitfalls of bisimulation-based represen-
 713 tations in offline reinforcement learning. *Advances in Neural Information Processing Systems*,
 714 36, 2024.
- 715 Yanjie Ze, Yuyao Liu, Ruizhe Shi, Jiaxin Qin, Zhecheng Yuan, Jiashun Wang, and Huazhe Xu.
 716 H-index: visual reinforcement learning with hand-informed representations for dexterous manip-
 717 ulation. In *Proceedings of the 37th International Conference on Neural Information Processing*
 718 *Systems*, pp. 74394–74409, 2023.
- 719 Yanjie Ze, Yuyao Liu, Ruizhe Shi, Jiaxin Qin, Zhecheng Yuan, Jiashun Wang, and Huazhe Xu.
 720 H-index: Visual reinforcement learning with hand-informed representations for dexterous manip-
 721 ulation. *Advances in Neural Information Processing Systems*, 36, 2024.
- 722 Amy Zhang, Rowan Thomas McAllister, Roberto Calandra, Yarin Gal, and Sergey Levine. Learn-
 723 ing invariant representations for reinforcement learning without reconstruction. In *International*
 724 *Conference on Learning Representations*, 2021.
- 725 Ruijie Zheng, Xiyao Wang, Yanchao Sun, Shuang Ma, Jieyu Zhao, Huazhe Xu, Hal Daumé III, and
 726 Furong Huang. TACO: Temporal latent action-driven contrastive loss for visual reinforce-
 727 ment learning. *Advances in Neural Information Processing Systems*, 36, 2024.
- 728 Qi Zhou, Jie Wang, Qiyuan Liu, Yufei Kuang, Wengang Zhou, and Houqiang Li. Learning robust
 729 representation for reinforcement learning with distractions by reward sequence prediction. In
 730 *Uncertainty in Artificial Intelligence*, pp. 2551–2562. PMLR, 2023.
- 731 Renzhe Zhou, Chen-Xiao Gao, Zongzhang Zhang, and Yang Yu. Generalizable task representation
 732 learning for offline meta-reinforcement learning with data limitations. In *Proceedings of the AAAI*
 733 *Conference on Artificial Intelligence*, volume 38, pp. 17132–17140, 2024.
- 734
- 735
- 736
- 737
- 738
- 739
- 740
- 741
- 742
- 743
- 744
- 745
- 746
- 747
- 748
- 749
- 750
- 751
- 752
- 753
- 754
- 755

756 Appendices

759 A PROOFS

761 A.1 THE PROOF OF LEMMA 4.3

762 **Lemma 4.3** (weak bisimulation metric). *The weak-bisimulation metric is a contraction mapping*
 763 *w.r.t the L^∞ norm on $\mathbb{R}^{\mathcal{S} \times \mathcal{S}}$, and there exists a fixed-point d_W^π for \mathcal{F}_W^π .*

765 *Proof.* To prove that the \mathcal{F}_W^π function has a fixed point d_W^π , we first need to prove that it is a
 766 contraction mapping.

768 As Definition 4.2, given the fixed expectation of $\epsilon(s_i, s_j)$, weak-bisimulation metric is,

$$770 \quad \mathcal{F}_W^\pi(d)(s_i, s_j) = \epsilon(s_i, s_j) - \gamma \mathcal{W}_1(d) \left(\mathcal{P}_{s_i}^\pi, \mathcal{P}_{s_j}^\pi \right) \quad (12)$$

772 Consider $d, d' \in \mathbb{M}$, we derive,

$$\begin{aligned} 773 \quad & |\mathcal{F}_W^\pi(d)(s_i, s_j) - \mathcal{F}_W^\pi(d')(s_i, s_j)| \\ 774 \quad &= \epsilon(s_i, s_j) + \mathcal{W}_1(d) \left(\mathcal{P}_{s_i}^\pi, \mathcal{P}_{s_j}^\pi \right) - \epsilon(s_i, s_j) - \mathcal{W}_1(d') \left(\mathcal{P}_{s_i}^\pi, \mathcal{P}_{s_j}^\pi \right) \\ 775 \quad &= \left| \gamma \left(\mathcal{W}_1(d) \left(\mathcal{P}_{s_i}^\pi, \mathcal{P}_{s_j}^\pi \right) - \mathcal{W}_1(d') \left(\mathcal{P}_{s_i}^\pi, \mathcal{P}_{s_j}^\pi \right) \right) \right| \\ 776 \quad &= \left| \gamma \sum_{s'_i, s'_j} \pi(a_i | s_i) \pi(a_j | s_j) \mathcal{P}_{s_i}^{a_i}(s'_i) \mathcal{P}_{s_j}^{a_j}(s'_j) (d - d')(s'_i, s'_j) \right| \\ 777 \quad &\leq \gamma \|d - d'\|_\infty. \end{aligned} \quad (13)$$

783 Therefore, $\mathcal{F}_W^\pi(d)$ is a contraction mapping w.r.t. the L_∞ norm and there exists a unique fixed-point
 784 d_W^π for $\mathcal{F}_W^\pi(d)$. \square

786 A.2 PROOFS OF THEOREM 4.4 AND THEOREM 4.5

788 Before proving Theorem 4.4 and Theorem 4.5, we need to present a weak assumption regarding
 789 the reward expectation under sparse reward settings. Then, we set the hyperparameter $\mu_c \geq$
 790 $|\mathbb{E}_{a_i \sim \pi} r_{s_i}^{a_i} - \mathbb{E}_{a_j \sim \pi} r_{s_j}^{a_j}|$, where μ_c is the mean of the trainable Gaussian distribution $\epsilon(s_i, s_j)$ in the
 791 weak bisimulation metric, i.e., $\mu_c = \mathbb{E}_{s_i, s_j \sim \mathcal{P}} [\epsilon(s_i, s_j)]$.

792 **Assumption A.1** (sparse-reward expectation). *Given a reward function $r_{s_i}^{a_i} = r(s_i, a_i)$ with sparse
 793 reward settings, the expectation of $r_{s_i}^{a_i}$ before obtaining the success reward satisfies $\mathbb{E}_{a_t \sim \pi} r_{s_t}^{a_t} \leq C_1$,
 794 where C_1 is a sufficiently small constant.*

795 Taking the verification environment of this work with sparse rewards as an example, experience
 796 shows that almost all transition rewards are usually minimal or even zero before reaching the goal.
 797 Therefore, the above Assumption A.1 is a weak assumption that is easy to satisfy in a sparse reward
 798 environment.

800 Then, based on the above weak assumptions, we can easily obtain,

$$802 \quad 0 \leq \left| \mathbb{E}_{a_i \sim \pi} r_{s_i}^{a_i} - \mathbb{E}_{a_j \sim \pi} r_{s_j}^{a_j} \right| \leq 2C_1. \quad (14)$$

804 In order to make $|\mathbb{E}_{a_i \sim \pi} r_{s_i}^{a_i} - \mathbb{E}_{a_j \sim \pi} r_{s_j}^{a_j}| \leq \mu_c$ hold, we only need to satisfy $C_1 \leq 1/2\mu_c$ in the
 805 actual implementation, where the hyperparameters C_1 and μ_c can be seen in Appendix C.2.

807 In light of the above conclusions, we then prove Theorem 4.4 and Theorem 4.5 respectively.

808 **Theorem 4.4** (Value difference bound). *Given states s_i and s_j , and a policy π , we have,*

$$809 \quad |V^\pi(s_i) - V^\pi(s_j)| \leq d_W^\pi(s_i, s_j) \quad (15)$$

810
 811 *Proof.* We follow the work (Castro, 2020) to prove the value function difference bound. To
 812 prove the above theory, we first introduce the standard value function $V_{n+1}^\pi(s_i) = \mathbb{E}_{a_i \sim \pi} r_{s_i}^{a_i} +$
 813 $\gamma \sum_{s' \in \mathcal{S}} \mathcal{P}_{s_i}^\pi(s') V_n^\pi(s')$ and the update operation with the property of contraction mapping (see
 Lemma 4.3),

$$d_{W,n+1}^\pi(s_i, s_j) = \epsilon(s_i, s_j) + \gamma \mathcal{W}_1(d_n^\pi) (\mathcal{P}_{s_i}^\pi, \mathcal{P}_{s_j}^\pi) \quad (16)$$

814 with initial $V_0^\pi \equiv 0$ and $d_{W,0}^\pi \equiv 0$.

815 Then, we proceed it by induction. For initial case $n = 0$, obviously $|V_0^\pi(s_i) - V_0^\pi(s_j)| \leq$
 816 $d_{W,0}^\pi(s_i, s_j)$ holds, and we then suppose true up to case n . Therefore, we have,

$$\begin{aligned} & |V_{n+1}^\pi(s_i) - V_{n+1}^\pi(s_j)| \\ &= \left| \mathbb{E}_{a_i \sim \pi} r_{s_i}^{a_i} + \gamma \sum_{s' \in \mathcal{S}} \mathcal{P}_{s_i}^\pi(s') V_n^\pi(s') - \left(\mathbb{E}_{a_j \sim \pi} r_{s_j}^{a_j} + \gamma \sum_{s' \in \mathcal{S}} \mathcal{P}_{s_j}^\pi(s') V_n^\pi(s') \right) \right| \\ &\leq \mathbb{E}_{a_i \sim \pi} r_{s_i}^{a_i} - \mathbb{E}_{a_j \sim \pi} r_{s_j}^{a_j} + \left| \gamma \sum_{s' \in \mathcal{S}} V_n^\pi(s') (\mathcal{P}_s^\pi(s') - \mathcal{P}_t^\pi(s')) \right| \\ &\leq \left| \mathbb{E}_{a_i \sim \pi} r_{s_i}^{a_i} - \mathbb{E}_{a_j \sim \pi} r_{s_j}^{a_j} \right| + \left| \gamma \mathcal{W}(d_{W,n}^\pi) (\mathcal{P}_{s_i}^\pi, \mathcal{P}_{s_j}^\pi) \right| \\ &= \left(\left| \mathbb{E}_{a_i \sim \pi} r_{s_i}^{a_i} - \mathbb{E}_{a_j \sim \pi} r_{s_j}^{a_j} \right| - \epsilon(s_i, s_j) \right) + \left(\epsilon(s_i, s_j) - \left| \gamma \mathcal{W}(d_{W,n}^\pi) (\mathcal{P}_{s_i}^\pi, \mathcal{P}_{s_j}^\pi) \right| \right) \\ &\leq \epsilon(s_i, s_j) + \left| \gamma \mathcal{W}(d_n^\pi) (\mathcal{P}_{s_i}^\pi, \mathcal{P}_{s_j}^\pi) \right| = d_{W,n+1}^\pi(s_i, s_j) \end{aligned} \quad (17)$$

817 where the second inequality comes from the dual representation of the Wasserstein distance (Villani,
 818 2021), and the last inequality is true when satisfying $C_1 \leq 1/2\mu_c$ based on the Assumption A.1.
 819 By the above steps, we can summarize that, $\forall n \in \mathbb{N}, \forall s_i, s_j \in \mathcal{S}, |V_{n+1}^\pi(s_i) - V_{n+1}^\pi(s_j)| \leq$
 820 $d_{W,n+1}^\pi(s_i, s_j)$ holds. \square

821 **Theorem 4.5** (relaxed value difference bound). *Given states s_i and s_j , and a policy π , we have,*

$$d_B^\pi(s_i, s_j) \leq d_W^\pi(s_i, s_j) \quad (18)$$

822 *Proof.* To prove $d_B^\pi(s_i, s_j) \leq d_W^\pi(s_i, s_j)$, we just need to prove $d_W^\pi(s_i, s_j) - d_B^\pi(s_i, s_j) \geq 0$.
 823 Clearly, given $C_1 \leq 1/2\mu_C$, we have,

$$\begin{aligned} & d_W^\pi(s_i, s_j) - d_B^\pi(s_i, s_j) \\ &= \left(\gamma \mathcal{W}_1(d) (\mathcal{P}_{s_i}^\pi, \mathcal{P}_{s_j}^\pi) + \epsilon(s_i, s_j) \right) \\ &\quad - \left(\left| \mathbb{E}_{a_i \sim \pi} r_{s_i}^{a_i} - \mathbb{E}_{a_j \sim \pi} r_{s_j}^{a_j} \right| + \gamma \mathcal{W}_1(d) (\mathcal{P}_{s_i}^\pi, \mathcal{P}_{s_j}^\pi) \right) \\ &= \epsilon(s_i, s_j) - \left| \mathbb{E}_{a_i \sim \pi} r_{s_i}^{a_i} - \mathbb{E}_{a_i \sim \pi} r_{s_i}^{a_i} \right| \geq 0 \end{aligned} \quad (19)$$

824 Then, $d_B^\pi(s_i, s_j) \leq d_W^\pi(s_i, s_j)$ holds. \square

B BACKGROUND SUPPLEMENT

B.1 BISIMULATION RELATION

825 Bisimulation Relations can be applied to group states in Markov Decision Processes (MDPs) that are
 826 behaviorally equivalent, aiding in state space reduction and efficient policy learning. Bisimulation
 827 Relation is defined as follows.

828 **Definition B.1** (Bisimulation Relations (Givan et al., 2003)). *Given an MDP $\mathcal{M} = (\mathcal{S}, \mathcal{A}, \mathcal{P}, r)$, a
 829 relation $E \subseteq \mathcal{S} \times \mathcal{S}$ is a bisimulation relation, if whenever $(s_i, s_j) \in E$ the following properties
 830 hold,*

$$\mathcal{R}(s_i, a) = \mathcal{R}(s_j, a) \quad \forall a \in \mathcal{A} \quad (20)$$

$$\mathcal{P}(G|s_i, a) = \mathcal{P}(G|s_j, a) \quad \forall a \in \mathcal{A}, \quad \forall G \in \mathcal{S}_B \quad (21)$$

831 where \mathcal{S}_E is the partition of \mathcal{S} defined by the relation E (the set of all groups G of equivalent states),
 832 and $\mathcal{P}(G|s, a) = \sum_{s' \in G} \mathcal{P}(s'|s, a)$.

864 **B.2 REPRESENTATIONS IN SPARSE REWARDS**
865

866 Reward signals can implicitly represent specific or abstract regions in observations that cause re-
867 wards (Yarats et al., 2021a). Recently, some work has modeled reward signals to obtain useful
868 representation information from observations, such as bisimulation metric representation based on
869 reward differences (Wang et al., 2024). However, when faced with real tasks with sparse rewards,
870 metrics tend to converge to the zero-fixed point due to continuous zero rewards, i.e., representa-
871 tion collapse (Liao et al., 2023). Although prior work has shown that modeling reward sequences
872 can collect richer reward signals (Kemertas & Aumentado-Armstrong, 2021; Yang et al., 2022), the
873 above problem is still difficult to avoid. Instead, it is more important to balance the dependence on
874 reward utilization in sparse reward environments.
875

876 **C IMPLEMENTATIONS**
877

878 **C.1 ACTOR-CRITIC**
879

880 Following the work Yarats et al. (2021b), we employ the Actor-Critic (AC) algorithm (Konda &
881 Tsitsiklis, 1999) as the backbone framework of DrQ-v2, where the DrQ-v2 is the basic structure of
882 the above experimental approaches. In general, AC is an off-policy reinforcement learning algorithm
883 for continuous control, consisting of a Critic network with a value function $Q_\vartheta(s_t, a_t)$ and an Actor
884 network with a policy function $\pi_v(s_t)$. Similar to Barth-Maron et al. (2018), this setting uniformly
885 uses the n -step return value to enhance the Temporal-Difference error estimation, and uses double
886 $Q_{k=0}$ and $Q_{k=1}$ to alleviate the overestimation bias. Therefore, we train the Critic network using
887 the following loss:
888

889
$$\mathcal{L}^Q(\vartheta_k, \phi_\omega) = \mathbb{E}_{\mathcal{D}} \left[Q_{\vartheta_k}(\phi_\omega(s_t), a_t) - \left(\sum_{i=0}^{n-1} \gamma^i r_{t+i} + \gamma^n \min_{k=0,1} Q_{\bar{\vartheta}_k}^{\text{tgt}}(\phi(s_{t+n}), a_{t+n}) \right) \right]^2 \quad (22)$$
890

891 where $Q_{\bar{\vartheta}_k}^{\text{tgt}}$ is the target Q function with frozen network parameters $\bar{\vartheta}_k$, and $\bar{\vartheta}_k$ is updated from the
892 exponential moving average (EMA) of the trainable parameters ϑ_k . \mathcal{D} represents the experience
893 replay buffer in off-policy DRL.
894

895 In addition, since DrQ-v2 adopts a deterministic policy, I train the Actor network with parameter v
896 with the following loss,
897

898
$$\mathcal{L}^\pi(v) = -\mathbb{E}_{\mathcal{D}} \left[\min_{k=0,1} Q_{\vartheta_k}(\phi_\omega(s_t), \pi_v(\phi_\omega(s_t)) + \varepsilon) \right] \quad (23)$$
899

900 where the action noise $\varepsilon \sim \text{clip}(\mathcal{N}(0, \sigma^2))$ is used to ensure the stochastic nature in the deterministic
901 policy. In the interactive phase, $\varepsilon \sim \mathcal{N}(0, \sigma_t^2)$, where σ_t is scheduled standard deviation for the
902 exploration noise. Notably, the encoder parameters ϕ_ω will not be trained by the Actor gradient, see
903 DrQ-v2 for details.
904

905 **C.2 HYPERPARAMETERS**
906

907 For the approaches involved in the experimental section, the main encoder network consists of 4
908 convolutional layers with the same filter sizes 3×3 and strides 2, 1, 1 and 1, respectively. In the
909 Actor and Critic networks, an encoder trunk network is independently set up to map the encoded
910 convolution output to a 50-dimensional feature vector, thereby serving the learning of policies and
911 value functions. For the settings of the SRL representation module, we set a 2-step transition dis-
912 tribution difference to achieve a trade-off between the utilization of the dynamics model and the
913 deviation caused by its accuracy. In addition, we set the sparse reward expectation $C_1 = 0.1$ in
914 Assumption A.1. To satisfy the condition $C_1 \leq 1/2\mu_c$, we conservatively set the mean $\mu_c = 0.5$
915 of the Gaussian distribution function $\mathcal{N}(\mu_c, \Sigma_\theta)$. It is worth noting that the replay buffer size in
916 this work is set to $2e^5$, which is 20% of the previous capacity. This can effectively verify the effi-
917 ciency of approaches while avoiding huge resource consumption. In fact, the experimental results
918 also show that the replay buffer size of $2e^5$ may be sufficient. Please see the table below for detailed
919 hyperparameters.
920

Table 3: Networks dimensions and hyperparameters.

Hyperparameter	Shared Setting
Training steps	$1 \sim 4M$
Seed frames	4000
Exploration steps	2000
Evaluation episodes	10
Replay buffer capacity	$2e^5$
Episode length	1000 for DMControl, 500 for MetaWorld, 200 for pen and 100 for hammer
Batch size	512 for walker_run and walker_walk, otherwise 256
Frame stack	1 for Adroit, otherwise 3
Discount factor γ	0.97 for MetaWorld, otherwise 0.99
State dims	$9 \times 84 \times 84$
Encoder conv kernels	[32,32,32,32]
Encoder conv filter size	$[3 \times 3, 3 \times 3, 3 \times 3, 3 \times 3]$
Encoder conv strides	[2,1,1,1]
Hidden dims	1024
Latent state dims	50
Action repeat	2
n -step returns	3
Optimizer	Adam
Learning rate	$1e^{-4}$
τ_Q	0.01
Gradient training frequency	2
Exploration temperature	0.1
Hyperparameter	SRL Setting
State transition step T	2
Sparse reward expectation C_1	0.1
Trainable Gaussian distribution mean μ_c	0.5

C.3 LEARNING ALGORITHM

We describe the main algorithm steps as follows.

Algorithm 1 Scalable Representation Learning (SRL)

```

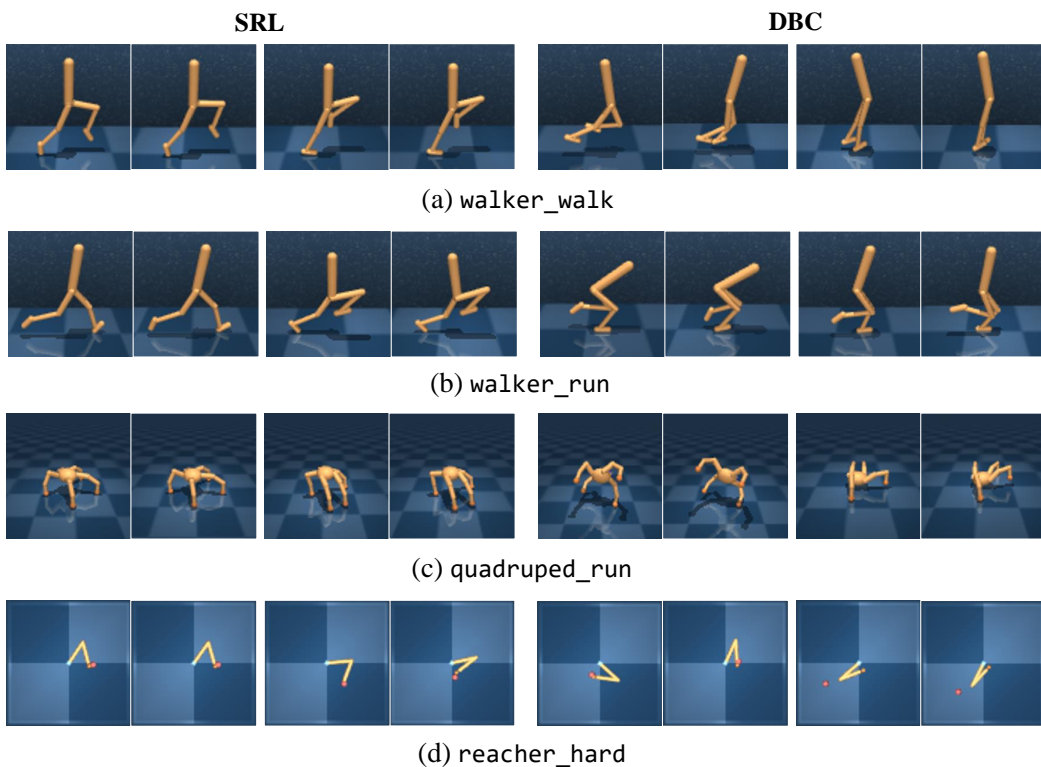
1: Initialize a replay buffer  $\mathcal{D}$  with size  $N$ , encoder  $\phi$ , policy  $\pi$ , latent model  $\hat{\mathcal{P}}_\psi$ .
2: for  $m \leftarrow 1$  to (# epochs) do
3:   for  $i \leftarrow 1$  to (# episodes per epoch) do
4:     Encode state  $z_t = \phi_\omega(s_t)$ 
5:     Execute action  $a_t \sim \pi_\phi(z_t) + \varepsilon$  where  $\varepsilon \sim \mathcal{N}(0, \sigma_t^2)$ .
6:     Run a step in environments  $s_{t+1} \sim \mathcal{P}(\cdot | s_t, a_t)$ 
7:     Collect data  $\mathcal{D} \leftarrow \mathcal{D} \cup \{s_t, a_t, r_{t+1}, s_{t+1}\}$ 
8:   end for
9:   for  $k \leftarrow 1$  to (# gradient steps) do
10:    Sample batch  $\mathcal{B}_i \sim \mathcal{D}$ 
11:    Rearrange batch  $\mathcal{B}_j = \text{Rearrange}(\mathcal{B}_i)$ 
12:    Sample a trainable Gaussian noise  $\tilde{\epsilon} = \mu_c + \sigma_1 f_\theta(\phi_\omega(s_j), \phi_{\bar{\omega}}(s_j))$ , where  $\sigma_1 \sim \mathcal{N}(0, 1)$ 
13:    Train encoder  $\mathbb{E}_{\mathcal{B}_i, \mathcal{B}_j} [\|\phi_\omega(s_i) - \phi_\omega(s_j)\|_2 - \mathcal{T}^{(T)}(s_i, s_j; \bar{\omega}, \theta)]$  with  $\hat{\mathcal{P}}_\psi^\pi$  in Equation (10)
14:    Train the Actor-Critic:  $\mathbb{E}_{\mathcal{B}_i} [\mathcal{L}^Q(\vartheta_{k=0,1}, \phi_\omega) + \mathcal{L}^\pi(\pi)]$  in Equation (22) and Equation (23)
15:    Train latent model  $\mathbb{E}_{\mathcal{B}_i} \|\hat{\mathcal{P}}_\psi^\pi(\cdot | z_t, a_t) - \bar{z}_{t+1}\|_2$  with frozen latent states
16:    Update target critics:  $\mathbb{E}_{\mathcal{B}_i} Q_{\vartheta_k}^{tgt} \leftarrow \tau_Q Q_{\vartheta_k} + (1 - \tau_Q) Q_{\vartheta_k}^{tgt}$ ,  $\forall k = 0, 1$ 
17:  end for
18: end for

```

972 D EXPERIMENTAL SUPPLEMENT
973974 D.1 THE BEHAVIOR SIMILARITY UNDER ENCODER SPACES
975

976 To quantitatively analyze the accuracy of the converged SRL and DBC encoders in terms of behav-
977 ior similarity metrics, we calculate the encoding distances $d = \|\phi_\omega(s_i) - \phi_\omega(s_j)\|_2$, ($0 \leq i, j <$
978 500) of their pairwise combinations over 500 states and show the two pairs of states with the small-
979 est encoding distance in Figure 8. It is worth noting that to avoid combinations with too close state
980 transition steps, we set $|i - j| \geq 250$ to ensure the effectiveness of the encoding distance.

981 As depicted in Figure 8, on the left and right sides, we display the two closest groups of encoded
982 distances for each DMC task under the SRL and DBC encoders, respectively. We can easily observe
983 that the two sets of encoding states with the closest distance identified by the SRL encoder, also have
984 very similar behavioral manifestation or task features intuitively. For example, in the walker_run,
985 the differences between the states in each group are almost indistinguishable. In contrast, although
986 the states classified by the DBC method have certain similarities, there are obvious differences in
987 the detailed behaviors, so the effect is not good enough. In summary, the above results show that the
988 weak bisimulation metric can effectively cluster similar states, and this ability actually requires SRL
989 to accurately extract task-relevant features in the state, which strongly proves that SRL has powerful
990 representation learning performance.



1016 Figure 8: Comparison of the behavioral similarity of state pairs under the latent space of SRL and
1017 DBC encoders. **Left:** SRL, **Right:** DBC.

1018 D.2 TASK-RELEVANT VISUALIZATIONS
1019

1021 As shown in Figure 9, we visualize the regions (green) of interest learned by convergent SRL and
1022 DBC encoders in the MetaWorld environment. Overall, we can observe that the features extracted
1023 by the SRL encoder (left side) are generally more complete and unambiguous. Interestingly, upon
1024 closer inspection, we notice that the SRL encoder may have also learned to recognize and emphasize
1025 potential safety boundaries, such as the operation boundaries on the desktop in the box-close
task. In contrast, the encoding abilities of DBC (right) are bad, as they either only notice partial

components (e.g., cups and pallets), while failing to capture potential task components (e.g., buttons and target points), or result in disorganized and unclear visualized regions, such as the `box-close` task. More importantly, the task relationships between components, the abstract features of logic, and the scope of the components themselves seem difficult to represent. Due to the lack of an overall understanding of the task, it is difficult for the DBC to perform each necessary operation in an orderly manner and complete the task. To sum up, SRL can more systematically and clearly extract the entity features and abstract features required to support decision-making tasks compared to the baseline, and demonstrates strong representation learning capabilities in sparse reward environments.

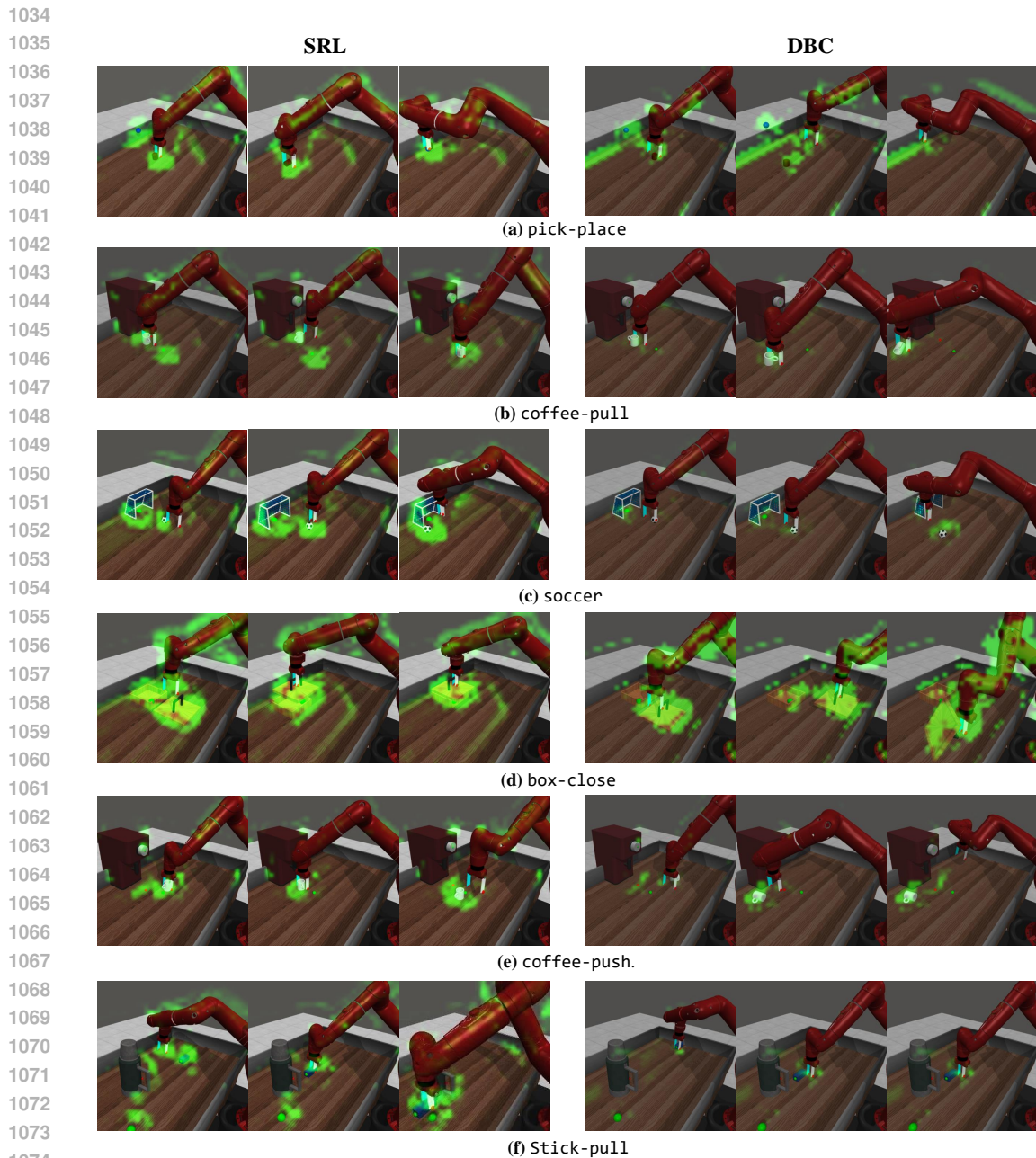


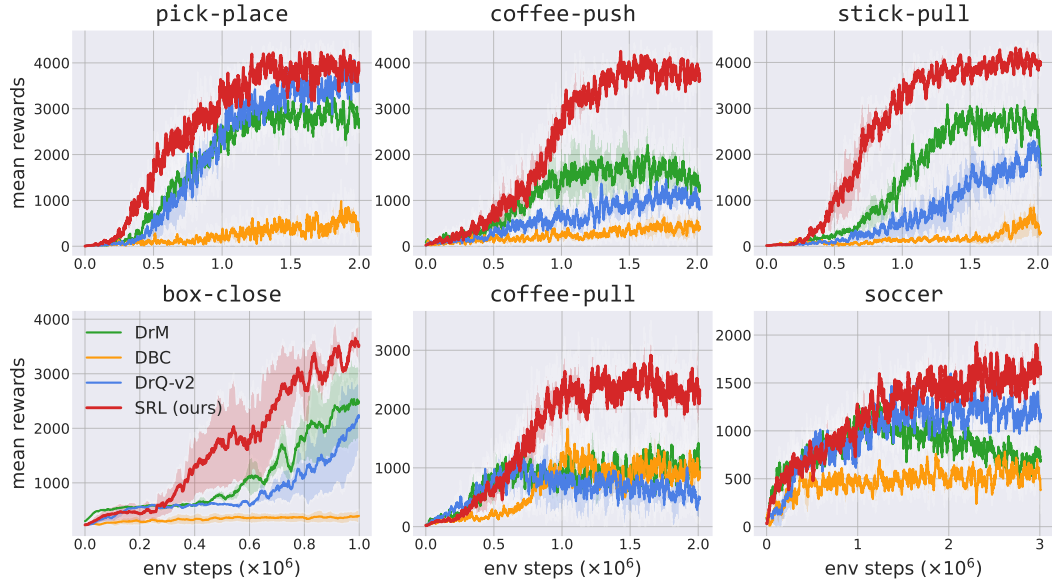
Figure 9: Visualization comparison between task-relevant features captured by the SRL and DBC encoders. **Left:** SRL, **Right:** DBC, with green heatmaps representing the task-relevant regions of interest as identified by the final convolutional layer of each encoder. Note that we employed consistent color parameters across both visualizations to ensure a fair comparison.

1080
1081

D.3 REWARD COMPARISON

1082
1083
1084
1085
1086
1087

As shown in Figure 10 and Figure 11, we report the comparison curves of mean episode rewards between SRL and baselines in the MetaWorld and Adroit environments, respectively. The highest episode reward results are recorded in Table 4. We can observe that, despite the difficulty of the task settings, our method achieves the highest rewards across all tasks. As a key baseline for bisimulation-based methods, DBC performed poorly in almost all tasks, and in some cases, it struggled to achieve dense rewards within the limited training frames.



1107

Figure 10: Learning curves of rewards for SRL and baselines on 6 complex tasks with sparse rewards in MetaWorld. Each curve represents the average of three random seeds, with the shaded regions indicating the standard deviation.

1108

1109

1110

1111

1112

1113

1114

1115

1116

1117

1118

1119

1120

1121

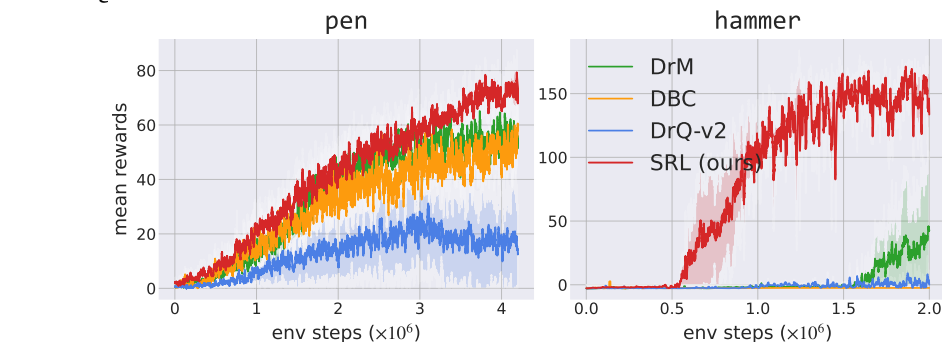
1122

1123

1124

1125

1126



1127

1128

1129

1130

1131

1132

1133

Figure 11: Learning curves of rewards for SRL and baselines on two complex tasks with sparse rewards in Adroit. Each curve represents the average of three random seeds, with the shaded regions indicating the standard deviation.

Table 4: Comparison results of the best mean episode reward on complex MetaWorld and Adroit tasks with sparse rewards.

Methods	pick-place	coffee-push	stick-pull	box-close	coffee-pull	soccer	pen	hammer
DrM	3345±80	2213±898	3091±168	2538±747	1424±253	1298±280	65.2±7.0	45.8±59.5
DBC	986±479	630±383	843±647	395±122	1665±58	784±241	60.6±3.7	2.7±0.0
DrQ-v2	4061±76	1460±59	2294±421	2242±788	1225±572	1598±168	31.2±20.0	9.1±13.6
SRL (ours)	4281±194	4254±73	4319±110	3650±203	2916±559	1925±211	79.4±8.0	171.3±13.6